IEEE Access
Multidisciplinary | Rapid Review | Open Access Journal

Received September 29, 2018, accepted November 17, 2018, date of publication November 28, 2018,
date of current version December 31, 2018.

Digital Object Identifier 10.1109/ACCESS.2018.2883733

Area-Averaged Transmitted Power Density at Skin Surface as Metric to Estimate Surface Temperature Elevation

DAISUKE FUNAHASHI[1], AKIMASA HIRATA[1], (Fellow, IEEE), SACHIKO KODERA[1], AND KENNETH R. FOSTER[2], (Life Fellow, IEEE)

[1]Department of Electrical and Mechanical Engineering, Nagoya Institute of Technology, Nagoya 466-8555, Japan
[2]Department of Bioengineering, University of Pennsylvania, Philadelphia, PA 19104, USA

Corresponding author: Akimasa Hirata (ahirata@nitech.ac.jp)

The work of D. Funahashi, A. Hirata, and S. Kodera was supported in part by the Ministry of Internal Affairs and Communications, Japan.

ABSTRACT In the international guidelines/standards for human protection, the specific absorption rate (SAR) is used as a metric to prevent excessive surface temperature elevation at frequencies up to 3 or 10 GHz. Above that transition frequency, including the frequency region assigned to 5th generation wireless communication systems, an area-averaged incident power density on human body surface is used as the physical quantity to specify the restrictions on human exposure to electromagnetic fields. However, the incident power density is an external physical quantity, resulting in frequency-dependent temperature elevation, which is attributable to frequency-dependent variations in the reflection coefficient at the skin surface and energy penetration depth into tissue. In this paper, we discuss analytically and computationally the effectiveness of the transmitted power density (TPD) at the skin as a new metric to estimate the steady-state skin temperature elevation above the transition frequency. We also consider simplified models for uniform and Gaussian beam patterns and the analytical solutions to the bioheat equation for an one-dimensional model, which are in good agreement with numerical solutions. These show that the TPD provides an excellent estimate of skin temperature elevation through the millimetre-wave band (30–300 GHz) and a reasonable and conservative estimate down to 10 GHz, whereas the SAR is a good metric below 3 GHz. Computational results for the dipole and patch antenna arrays demonstrated that the one-dimensional analysis is conservative metric as compared with the TPD averaged over the area of 4 cm^2 (2-cm square). Considering extreme cases, averaging area smaller than 4 cm^2 is needed above 30 GHz for beam exposure with small diameters. Finally, we consider the choice of averaging area as related to peak temperature increases for small beams. For extremely small exposure areas, limits on peak power density may be needed.

INDEX TERMS Human safety, dosimetry, standardization.

I. INTRODUCTION

There are two international guidelines/standard for human protection from electromagnetic field (below 300 GHz) set forth as recommendation by World Health Organization: the International Commission on Non-Ionizing Radiation Protection (ICNIRP) [1] and the IEEE International Commission on Electromagnetic Safety (ICES) [2], [3]. The guidelines (the designation used by ICNIRP) /standard (IEEE) are presently undergoing revision; in the ICNIRP guidelines over frequency range from 100 kHz to 300 GHz and in the IEEE standard from 0 kHz to 300 GHz.

For human protection against thermal hazards, both limits are defined in terms of the specific absorption rate (SAR) averaged over 10 g of tissue for frequencies up to 3 GHz [2] or 10 GHz [1]. The metric is considered as a surrogate of local temperature elevation. Above the transition frequencies of 3 or 10 GHz, both limits use the incident power density (IPD) averaged over a specific area as a metric for exposure. While the choice of the optimal volume over which to average SAR has been extensively discussed [4]–[7], there has been much less consideration of optimal averaging area. Present versions of the limits specify averaging areas that

TABLE 1. Parameters of dipole antenna and cube of the human model composed of homogeneous skin at different frequencies.

Frequency [GHz]	0.3	0.5	0.8	1	1.5	2	3	4	5	6	8	10	15	20	30	40	60	80	100	150	200	300
Length of the antenna [mm]	496	302	186	144	94	70	49	35	28	23	17	13	9	6.5	4	3.3	2	1.5	1.3	0.8	0.6	0.45
Resolution [mm]	1						0.5						0.25			0.125			0.05			0.025
Depth of the model [mm]	200						100						75			50			30			15
Side length of the model [mm]	400						200						150			100			60			30

are frequency dependent [2] and fixed at 20 cm^2 [1]. Recent studies suggest that an appropriate averaging area would be 2 to 4 cm^2 based on thermal analysis of heat transfer (thermal conduction and convection by blood perfusion) in tissues [8], [9]. This averaging area approximately coincides with a face of the volume for the averaging mass of 10 g for local SAR.

The limit on SAR does not depend on the frequency because it is expressed in terms of an internal physical quantity (dose). The SAR behaves as a heat source and the averaging volume approximately corresponds to a combination of the thermal diffusion length and a screening distance due to convective cooling by blood flow. Even though the limit of IPD is constant above the transition frequency (3 or 10 GHz), the power transmitting to the tissue and energy penetration depth both depend on the frequency (e.g. [8]–[10]). However, as discussed below, at millimeter (mm)-wave frequencies the heat load at the surface is a good predictor of the elevation in skin temperature, and a reasonable approximation down to about 10 GHz. In addition, Hashimoto *et al.* [9] showed that the skin temperature elevation can be approximately derived from the absorbed power in the surface (IPD multiplied by transmission coefficient) which is a measure of heat load at the surface. However, these results apply for plane waves incident on the surface. Even above the transition frequency (especially around the transition frequency), the interaction between the antenna and the body may not always be neglected.

The purpose of this study is to discuss a new metric or internal physical quantity for estimating surface temperature above the transition frequency. The metric 'transmitted power density (TPD) to the skin surface' or 'epithelial power density' is proposed based on analytic and computational approaches. This metric has already been mentioned in the ICNIRP public consultation document and IEEE C95.1 draft based on an extrapolation of the authors' study [8], [9]. First, an analytic solution is presented for a highly simplified model that suggests why the TPD should be a useful estimate of the surface temperature elevation in the steady state. More detailed computational examples are provided in this contribution to demonstrate the effectiveness of this approach for dipole antenna and 4-element dipole and patch antenna arrays.

II. COMPUTATIONAL METHODS AND HUMAN MODEL

A. SKIN AND HUMAN BODY MODELS

A three-dimensional homogeneous cube with thermal and electrical parameters similar to those of skin was considered for analysis. The dimensions of the cube are listed in table 1.

In order to confirm the finding obtained from the cube, we also considered realistic human models, Japanese male model named TARO [11], which has been developed from magnetic resonance images. This model is comprised of more than 50 tissues/organs, such as skin, muscle, bone, and so on. In addition to these two models, homogeneous (skin) model with the same shape as realistic human models was also considered. An in-house smoothing algorithm was applied to refine higher resolution models of TARO [12].

B. ELECTROMAGNETIC ANALYSIS

The finite-difference time-domain method (FDTD) [13] was used to conduct electromagnetic dosimetry in a human model exposed to high-frequency fields emitted from electromagnetic source. The SAR is defined as

$$SAR\left(\boldsymbol{r}\right) = \frac{\sigma\left(\boldsymbol{r}\right)}{2\rho\left(\boldsymbol{r}\right)}\left|\boldsymbol{E}\left(\boldsymbol{r}\right)\right|^2, \tag{1}$$

where $|\boldsymbol{E}(\boldsymbol{r})|$ is the peak value of the electric field at position $\boldsymbol{r}$, and σ and ρ are the conductivity and mass density of the tissue, respectively.

In addition to the SAR, TPD is defined as

$$TPD\left(x, y\right) = \frac{1}{2}\int \sigma\left(\boldsymbol{r}\right)\left|\boldsymbol{E}\left(\boldsymbol{r}\right)\right|^2 dz, \tag{2}$$

where z is the direction perpendicular to the body surface. The TPD corresponds to the SAR integrated over the depth direction.

The dielectric properties of the tissues were determined with a four-Cole–Cole dispersion model [14], where the upper frequency at which the measured data were considered is 20 GHz. Its extrapolated data is used. Measurement and its discussion at higher frequencies has been conducted recently [15]–[17].

C. THERMAL ANALYSIS

A computational method for the temperature elevation is identical to that in our previous study [18]. The temperature in

the human model is computed by solving a bioheat transfer equation [19]. The equation, which takes into account heat exchange mechanisms, i.e., heat conduction and blood perfusion, and electromagnetically induced heating (SAR), is represented by the following equation:

$$C(\boldsymbol{r})\,\rho(\boldsymbol{r})\,\frac{\partial T(\boldsymbol{r},t)}{\partial t} = \nabla\cdot(K(\boldsymbol{r})\,\nabla T(\boldsymbol{r},t)) + \rho(\boldsymbol{r})\,SAR(\boldsymbol{r}) + M(\boldsymbol{r},t) - B(\boldsymbol{r},t)\,(T(\boldsymbol{r},t) - T_B(\boldsymbol{r},t)) \quad (3)$$

where T is the temperature of the tissue, T_B is the blood temperature, C is the specific heat of the tissue, K is the thermal conductivity of the tissue, M is the metabolic heat generation, B is the term associated with blood perfusion, and t is the time variable. The blood temperature is assumed to be spatiotemporally constant in the same tissue because exposure scenarios considered (see below) are local, which is insufficient to cause core temperature elevation; generally negligible as compared to the basal metabolism (−100 W). Hence, the blood temperature $T_B(\boldsymbol{r},t)$ in (3) is treated as constant (37 °C). The boundary condition for (3) is given by

$$-K(\boldsymbol{r})\,\frac{\partial T(\boldsymbol{r},t)}{\partial \boldsymbol{n}} = H\cdot(T_s(\boldsymbol{r},t) - T_e(t)), \quad (4)$$

where H, T_s, and T_e denote the heat transfer coefficient, skin temperature, and ambient temperature (independent of the position), respectively. The variable $\boldsymbol{n}$ denotes the axis perpendicular to the model surface. In the frequency range of chief interest here, > 6 GHz, the heating is confined to a thin (mm or less) layer near the surface [8], and heat transport is chiefly by means of thermal conduction due to the large temperature gradients near the surface.

First, the bioheat transfer equation subjected to the boundary condition was solved to obtain the thermal steady-state temperature. The left-hand-side of (3) was then equated to be zero to obtain the steady state temperature elevation. The equation was discretised using a finite difference method and solved by applying the geometric multi-grid method [20].

Most thermal parameters used in this study are the same as those used in [4], wherein the parameters were borrowed primarily from the study conducted by [21]. The blood flow in the skin tissue was taken from [22]. As discussed in [23], the blood flow varies substantially in a shallow region (from skin surface to 3 mm), but its impact on the steady-state surface temperature elevation is ±15% at frequencies higher than 6 GHz, which is consistent with Monte-Carlo approach [10]. Also, possible thermoregulatory changes in skin blood flow are ignored since they are known to be minor for local increases in skin temperature (in the absence of increases in core temperature) below 1-2 °C (see the discussion in [24]).

D. SIMPLE ANALYTICAL MODEL

Analytical solution in [25] is reviewed briefly. Solutions to (3) for a variety of cases are known but are mathematically complex. For purposes of comparison we consider a highly oversimplified "baseline" model assuming adiabatic boundary conditions (no heat lost to the environment) and plane wave radiation normally incident on a planar tissue surface with uniform thermal and electrical properties. The SAR produced by exposure is then

$$SAR = \frac{I_o T_{tr}}{\rho L} e^{-z/L} = SAR_o e^{-z/L} \quad (5)$$

where I_o is the incident power density on the tissue, T_{tr} is the energy transmission coefficient into the plane and L is the energy penetration depth into tissue, which is defined as the distance beneath the surface at which the SAR has fallen to a factor of $1/e$ below that at the surface. L is one-half of the more commonly reported wave penetration depth. Analytical expressions for the transient and steady state increase in this 1D model can be obtained readily by computer algebra (Maple, Waterloo Maple, Waterloo ON) but are lengthy and not repeated here; they are provided in [26].

An even simpler approximation is to consider heating to occur at the surface only (the surface heating approximation). This is a reasonable approximation at mm wave frequencies, where the energy penetration depth in skin ranges from 0.1-0.4 mm. This model assumes that the SAR is zero within the tissue and models the surface heating through the boundary condition at the surface:

$$\frac{\delta T}{\delta z} = -\frac{I_o T_{tr}}{k} u(t) \quad (6)$$

where $u(t)$ is the unit step function to indicate that exposure begins at t=0. Equation (6) is readily solved (using Maple) after transforming to the Laplace domain. The transient increase in temperature at the surface $T(0,t)$ is

$$T(0,t) = \frac{I_o T_{tr}}{\sqrt{kB}} erf\left(\sqrt{\frac{t}{\tau_1}}\right)$$

where

$$\tau_1 = \frac{\rho C}{B} \approx 500 \text{ sec} \quad (7)$$

Using the thermal parameters presented above, this corresponds to a steady state temperature increase at the surface of

$$T_{ss} \approx 0.018 I_o T_{tr} \quad (8)$$

This implies a heating factor of ≈ 0.02 °C·m^2/W independent of frequency. Analytical solutions for the 1D model for finite energy penetration depth are presented in [25]. They show that as the energy penetration depth increases (lower frequencies) the steady state temperature at the surface of the tissue decreases for a given absorbed energy density. However, the errors introduced by the surface heating approximation are only modest above the transition frequency, approximately 25% overestimate in temperature at 10 GHz and much smaller in the mm wave band (30-300 GHz).

Apart from its assumption of a homogeneous tissue, this 1D model allows thermal conduction only in a direction

normal to the tissue surface and consequently will overestimate the heating effects from finite sources. The following discussion considers several examples.

The case of finite exposed areas can be modelled by assuming that exposure occurs uniformly over a disk of radius Ro (a 2D model with rotational symmetry). The maximum temperature increase in the steady state for this model, assuming purely surface heating, can be written as [8], [25]

$$T^{ss}_{uniform} = \frac{I_o T_{tr} R_1}{k}\left(1 - e^{-x}\right)$$
Uniformly irradiated area (9a)

$$T^{ss}_{Gaussian} = \frac{I_o T_{tr} R_0 x\sqrt{\pi}}{2k} e^{x^2/4}\left(erf\left(x/2\right) - 1\right)$$
Gaussian beam pattern (9b)

where

$$x = R_0/R_1 \quad (9c)$$

$$R_1 = \sqrt{\frac{k}{B}} \approx 7 \text{ mm}. \quad (9d)$$

This approximation is valid for short-penetrating radiation (mm-waves), and will overestimate the temperature increase at lower frequencies. This indicates that for disks greater than about 1 cm radius, the ratio $\Delta T/(I_o T_{tr})$ will approach R_1/k, or 0.03 °C, falling to R_0/k for smaller disks. Consequently the steady state temperature rise will be roughly independent of the exposed area if its dimensions are a cm or larger. As stated above this approximation assumes near-surface heating, and will overestimate the temperature increase below the mm wave range. This result is easily extended to the more realistic case of a Gaussian exposure pattern [25].

E. EXPOSURE SCENARIOS

Fig. 1 shows the exposure scenarios considered in this study: the half-wave dipole antenna and four-element dipole and patch antenna arrays. The lengths of the antenna were adjusted such that they would resonate at the corresponding frequencies. Resultant parameters are listed in Table 1. The parameters of patch antenna array are shown in Fig. 2 and table 2. Patch antenna array is located so that the field is emitted to the opposite direction from the human.

TABLE 2. Parameters of patch antenna array at different frequencies.

Frequency [GHz]	10	15	20	30	40	60	80	100
Thickness of substrate (D) [mm]	0.75				0.375			
Side length of elements (L) [mm]	9.0	6.0	4.5	3.0	2.25	1.5	1.0	0.75
Resolution [mm]	0.25				0.125			
Depth of the model [mm]	75				50			
Side length of the model [mm]	150				100			

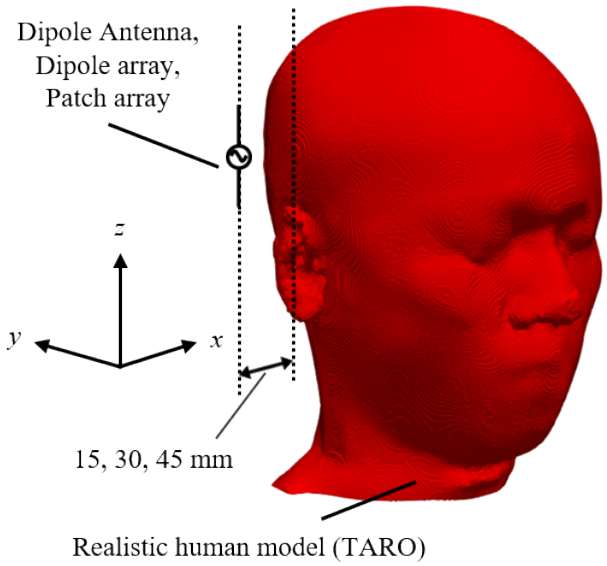

FIGURE 1. Exposure conditions of bird's-eye view for a dipole antenna, four-element dipole and patch antenna arrays. The distance between the neighboring antennas in the array is one half-wavelength corresponding to the respective frequencies.

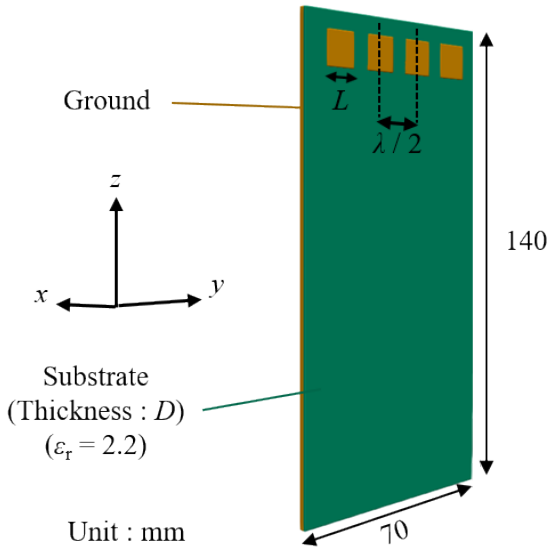

FIGURE 2. Geometry of patch antenna array on the dielectric substrate. The distance between the neighbouring antennas in the array is one half-wavelength corresponding to the respective frequencies.

Commercial communications systems at frequencies above 6 GHz have not yet been widely introduced to market, although a variety of transmitters, both for base stations and for mobile phone handsets have been developed (e.g., [27], [28]). The following discussion considers some simplified antenna and antenna arrays of the sort that may be used in future handsets. The separation distances between the model surface and the antenna, or the antenna array were chosen to be 15, 30, and 45 mm as shown in Fig. 1. In the antenna array, the separations between the neighbouring antennas are chosen to be half of the wavelength corresponding to the given frequency.

F. METRICS FOR EVALUATION

SAR averaged over 10 g of tissue and IPD are considered as metrics as prescribed in the guidelines and standard. In addition to these two metrics, the TPD at the surface is also evaluated. The IPD is defined as the magnitude of the Poynting vector in free space at the separation distance between the antenna and the model surface; closest distance in case of anatomical model. The physical quantity TPD is power deposition integrated over the depth direction from the surface, as shown in (2), and can be approximately obtained by multiplying a transmission coefficient by IPD. The IPD is averaged over area of 4 cm^2 and 1 cm^2 (in square shape) on the plane where the model surface exists, which are in the range of a draft ICNIRP guideline (public consultation; 11 July 2018) and IEEE standard C95.1; they have been also discussed in Global Coordination of Research and Health Policy on RF Electromagnetic Fields (Washington DC, Dec. 2017). TPD were computed by averaging over the same areas on the skin surface. When considering anatomical human models, the model surface may not be flat. The TPD was then projected on the plane where the IPD averaging plane exists.

We introduced a heating factor defined as the spatial-peak steady-state temperature elevation in the head divided by the IPD and TPD averaged over specific areas or SAR averaged over 10 g of tissues. Once these values are obtained, the peak steady-state temperature elevation can be estimated by multiplying the corresponding values to the limit. The position where the peak temperature elevation appear is the surface above 6 GHz, but at lower frequencies it may be below the skin surface including in muscle. All heating factors are calculated in terms of steady state temperature increases, which require times of the order of minutes to be achieved after exposure is begun.

III. COMPUTATIONAL RESULTS

A. TRANSMITTED POWER AND STEADY STATE TEMPERATURE ELEVATION IN 1-D SKIN MODEL

The heating factor for SAR averaged over 22-mm depth (corresponding to 10 g of tissue in the 3-D model), IPD, and TPD are computed in 1-D skin model, in addition to analytical solution presented in Sec. II. In the analytical solution, IPD and TPD are defined as I_o and $I_o T_{tr}$, respectively. As shown in Fig. 3, the computational (numerical) results of Nagoya Institute of Technology for the one-dimensional model agree quite well with analytical solutions and FEM computation by K. Foster to the bioheat equation (see (3)) over the entire frequency range. The numerical and analytical results also converge to results of the surface heating model (see (8)) above 30 GHz. In a more complex tissue model [25], thermal resistance of subcutaneous tissues, principally fat, will result in increases in surface temperature higher than in (3) which assumes a homogeneous tissue.

The heating factor for SAR ($\Delta T/SAR$) is frequency independent below 3 GHz, but increase with increasing frequency above 3 GHz. The heating factor for IPD ($\Delta T/IPD$) increases with the increase of the frequency over the frequency range. SAR and TPD are good metrics to estimate the skin temperature elevation for frequencies below 3 GHz and above 10 GHz, respectively.

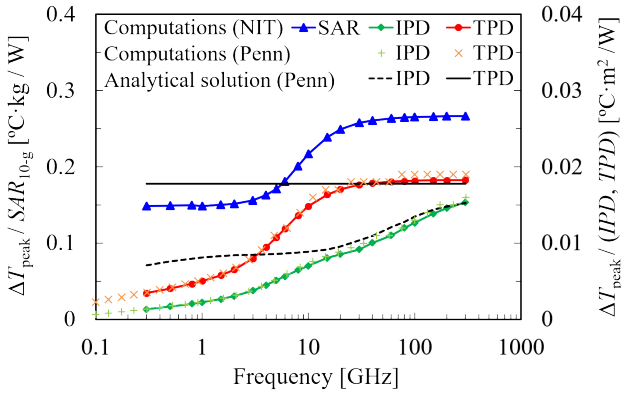

FIGURE 3. The ratio of the surface temperature elevation to the SAR, IPD and TPD (the heating factor) for the one-dimensional model (i.e. assuming plane wave exposure that is uniform over the entire tissue boundary). FDTD computed and analytical solution of the bioheat equation considering finite energy penetration depth (8) were shown for comparison.

All of these heating factors increase with frequency because of two factors: the general increase in transmission coefficient T_{tr} with frequency, and the general increase in steady state temperature rise with frequency that results from decreasing penetration depth. Both effects become less frequency dependent in the mm wave range (30-300 GHz). Because the TPD is not dependent on the T_{tr} it is generally less variable with frequency. Moreover, in the mm wave band the thermal response is closely approximated by the surface heating model, which is independent of penetration depth.

B. HEATING FACTOR FOR SAR, IPD AND TPD AT THE SKIN SURFACE IN 3-D SKIN MODEL

Fig. 4 shows the frequency dependence of heating factors for SAR, IPD and TPD calculated for the dipole antenna. These quantities were averaged over (a) 4 and (b) 1 cm^2 and refer to steady state temperature increase. These show generally similar frequency dependence as in the 1D model. The heating factors calculated for exposure from the dipoles are generally somewhat smaller than for plane wave exposures because the IPD, TPD, and SAR are averaged over a nonuniform absorption pattern whose extent varies with antenna size (or alternatively frequency). In addition, the exposures at the lower frequencies were in the near fields of the antennas and electrical interactions between the antenna and model can be significant. Overall, these results with finite sources are remarkably similar to results from the simple 1D model. In addition, the TPD averaged over 4 cm^2 are rather frequency independent. The difference in the heating factor for TPD at 30 and 300 GHz are less than 15% for the averaging area of 4 cm^2. The heating factors for TPD at 6 and 10 GHz were

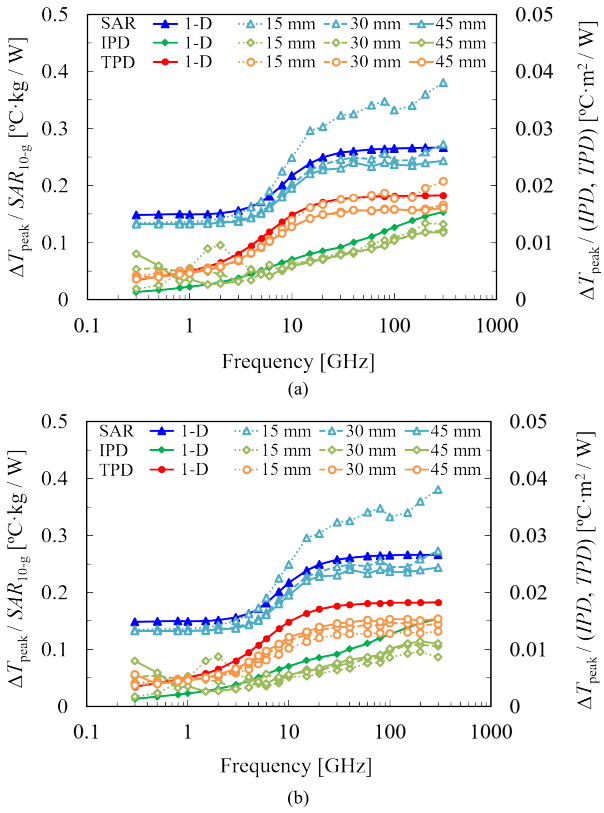

FIGURE 4. The ratio of the surface temperature elevation to the SAR, IPD and TPD (the heating factor) for the dipole antenna. The SAR was averaged over 10 g cubes, while the IPD and TPD were averaged over (a) 4 cm^2, (b) 1 cm^2.

49% and 33% of that at 300 GHz (which is chiefly an effect of a lower energy transmission coefficients into tissue at the lower frequencies).

As shown in Fig. 4 (b), the heating factor of the IPD and TPD averaged over 1 cm^2 calculated for dipole antennas are approximately 21% and 16% smaller than that of the one-dimensional analysis results, respectively. This is chiefly attributable to thermal conduction in direction parallel to the skin surface (which is not present in the 1D model). This effect becomes more significant as the exposed area is reduced below about 1 cm^2 [26], [29]. For the smaller dipoles, the heating factor $\Delta T/TPD$ is approximately in agreement with that predicted by the simple approximation (see (9)). It implies that the temperature increase is chiefly limited by heat conduction from the exposed area, due to the relatively high thermal gradients near the exposed region.

C. HEATING FACTOR FOR TPD FOR DIFFERENT ANTENNAS AND HUMAN MODELS

Fig. 5 shows the frequency dependence of heating factors for TPD emitted from the four-element dipole antenna and patch antenna array. Two averaging areas of 4 cm^2 and 1 cm^2 were considered, similar to that in the above subsection. As shown in Fig. 5, heating factors for the dipole antenna array are

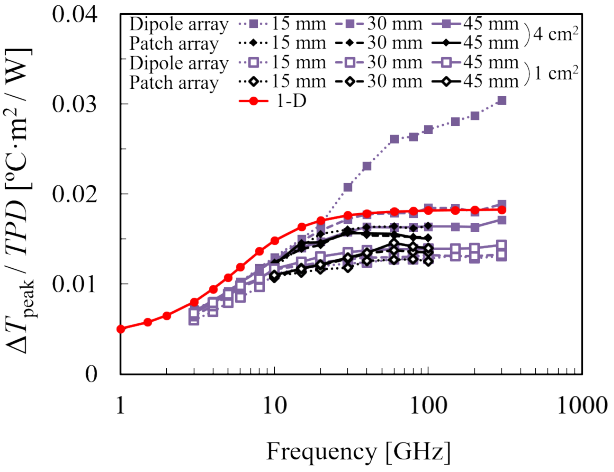

FIGURE 5. The ratio of the surface temperature elevation to the TPD averaged over 4 cm^2 and 1 cm^2 for the four elements dipole antenna and patch antenna array.

similar to those from the dipole antenna below 30 GHz. Above that frequency range, whereas the heating factor for patch antenna array is conservative to one-dimensional model up to 100 GHz, the beam diameter of the dipole antenna array becomes smaller than the side length of the averaging area of 4 cm^2 with the increase of the frequency especially prominent at antenna separations of 15 mm; for example, shorter axis of the beam from dipole antenna array at 30 GH is 13.5 mm, 18 mm, and 26 mm at the distance of 15 mm, 30 mm, and 45 mm. For an averaging area of 1 cm^2, the heating factors of TPD are frequency independent and smaller than for the one-dimensional model. This arises in large part due to heat conduction in a direction parallel to the tissue surface, which does not occur in the 1D planar model (where heat conduction occurs only in the normal direction to the surface).

To confirm the difference due to the size of the averaging area, the relation between the heating factor for TPD averaged over 4 cm^2 and the beam area is presented in Fig. 6 for the dipole antenna and antenna array. The beam area was defined as the area whose local TPD is larger than $1/e$ of the maximum value. Also shown is the calculated temperature increase for a uniformly exposed disk (''Gaussan beam (see (9b))'' in the Fig. 6). For beam areas larger than a few square centimeters, the heating factor becomes nearly independent of the area.

The heating factor associated with the dipole antenna was assessed in the head of the anatomically detailed model TARO and the homogenized head model in Fig. 7. Computed results in averaging area of 4 cm^2 were plotted in addition to the 1-D and homogeneous cube curves. As shown in Fig. 7, the realistic models show similar heating factors as for the planar and cubic models. However, the heating factor for the TARO is higher than that for the cube by 10-21%. This difference is due in part to the parameter of blood flow in subcutaneous tissue [23].

The exposure limits do not directly control the output power of antennas near tissue surface, but the power is

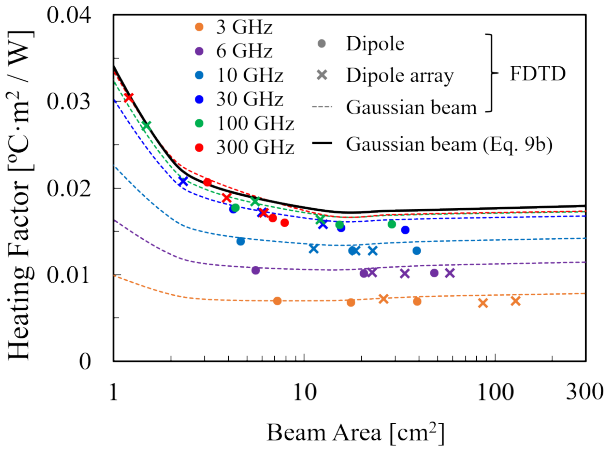

FIGURE 6. The heating factor for TPD averaged over 4 cm^2 for dipole antenna and dipole antenna array in a homogeneous planar model. Beam area was defined as the area whose TPD is larger than 1/*e* of the maximum value. The solution (see (9b)) for a Gaussian exposed disk of radius corresponding to the beam area is shown. Also shown are FDTD solutions for ideal Gaussian beam at different frequencies for comparison. FDTD computation was conducted assuming the adiabatic condition for comparison with analytical solutions. The FDTD solution for the Gaussian disk model is almost equal to the analytical model.

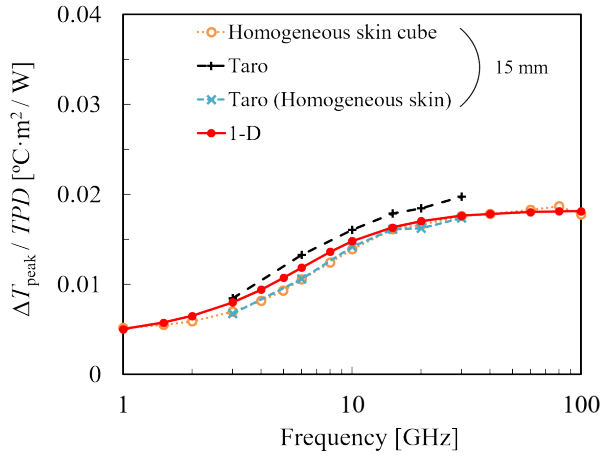

FIGURE 7. The ratio of the surface temperature elevation to the TPD (the heating factor) for the dipole antenna in anatomical human model. The averaging area of TPD was 4 cm^2.

indirectly controlled through the limits on basic restrictions. Fig. 8 shows the maximum permissible output power compliant with TPD limits of draft ICNIRP and IEEE limits from dipole antennas and antenna arrays at the distance of 15 mm from the tissue surface. As shown in Fig. 8, the maximum permissible power radiated from the half-wave dipole antenna decreases gradually with increasing the frequency up to a few GHz. Then it is almost frequency independent; for example, the difference of the maximum permissible power from resonant dipole antennas separated from the tissue surface by 15 mm was 21.9, 20.4, and 18.7 dBmW at 6, 30, and 100 GHz. However, maximum permissible power from dipole antenna array decreases with the increase of the frequency because of the smaller beam diameter at higher frequencies.

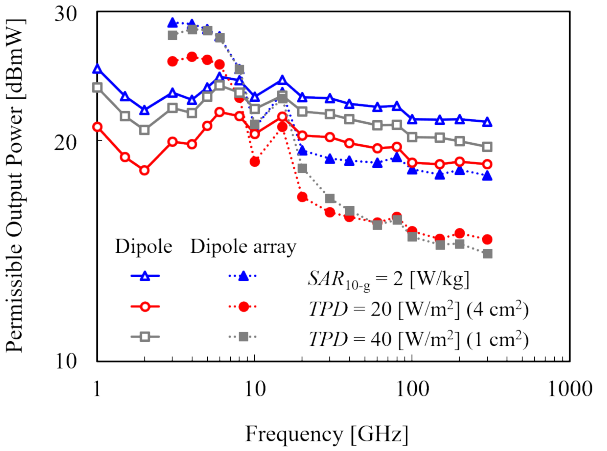

FIGURE 8. Permissible output power for dipole antenna and dipole antenna array when SAR or TPD restricted to the exposure limit.

IV. DISCUSSION AND CONCLUDING REMARKS

The analytical and numerical solutions for the different models reviewed above show that the TPD is good metric to estimate the maximum (skin) temperature elevation at mm-wave band (above 30 GHz). The steady state temperature increase from exposures to sources located close to the body surface is generally smaller than from plane wave exposure at the same peak TPD due to heat diffusion parallel to the skin surface. However, for very near-field exposures (antennas much less than a wavelength from the body surface), coupling effects to the body become important (e.g., see Fig. 10 (b)).

The problem of exposure to beams of small area raises the issue of proper choice of averaging area in the guidelines. Both ICNIRP and IEEE limits specify averaging areas (1 cm^2 from 30-300 GHz in proposed guidelines).

The concept of averaging area implicitly assumes that the exposure is calculated as a running average of IPD or TPD over the averaging area. That is perhaps adequate for most exposures. However, a more mathematically correct approach would require convolving the Green's function for the bioheat equation with the TPD [25]. Because the Green's function is sharply peaked at small distances [25, (A11)], a simple area average of exposure will be a poor predictor of temperature increase if the exposure is strongly nonuniform. That will be the case for many of the exposures considered here that result in small beam areas. If the beam intensity is constrained by the requirement that the TPD is less than a fixed amount when averaged over a finite area, that could potentially allow very high peak TPD for very small area beams and possibly excessive temperature elevation.

To evaluate this effect, we extend the analysis used for Fig. 6 to very small beam areas, using the approximate models for uniformly and Gaussian beams in the surface heating approximation (see (9a, b)). If we assume that the averaging area is a circle of radius R_{av}, the allowable TPD for large-area exposures is I_o, and the beam area impinging on the skin has a radius R_0, the maximum allowable TPD over the beam will be $I_o\ (R_{av}/R_0)^2$, where $R_0 \leq R_{av}$ or I_o for $R_0 \geq R_{av}$. The

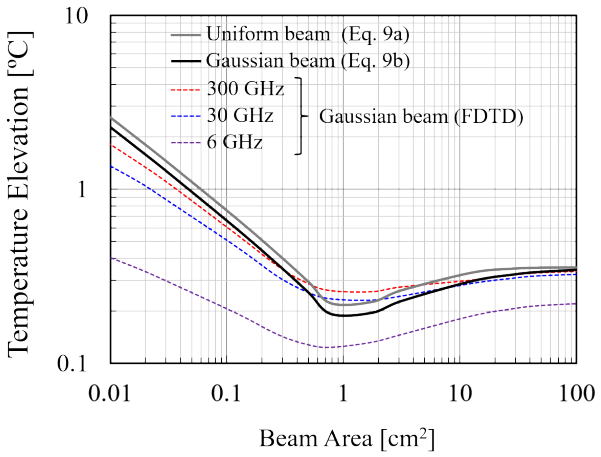

FIGURE 9. Steady state temperature increases in uniformly and Gaussian disk models as function of disk area surrounded by unexposed skin. The peak TPD was adjusted to maintain average TPD over 1 cm^2 equal to 20 W/m^2, corresponding to proposed ICNIRP basic restrictions 30-300 GHz. The calculations for the uniform and Gaussian beams (see (9a, b)) assumed purely surface heating, while the FDTD calculations were based on finite energy penetration depths appropriate for the indicated frequency. FDTD computation was assumed the adiabatic condition for comparison with analytical calculations.

peak increase in steady state temperature in the two models is easily found from (9a, b) (see Fig.9).

Fig. 9 shows the peak temperature increases from these two models, calculated assuming I_o = 20 W/m^2(proposed basic restrictions for the general public, 6-300 GHz), and R_{av} = 5.6 mm (for an averaging area of 1 cm^2). The transmission coefficient was T_{tr}=1 to provide the TPD. The results (Fig. 9) show that the peak temperature increases can exceed 1 °C for small beam areas ($<\approx 0.08$ cm^2). This peak increase could be a factor of 5 higher for occupational limits, and could be as much as another factor of 4 higher below 30 GHz (assuming that energy is accumulated over an averaging area of 4 cm^2 and deposited in a much smaller area) and exceed thresholds for thermal pain ($\approx$ 8 °C above normal skin temperature).

The practical consequence of this increase in peak temperatures for small exposure areas is unclear for several reasons: (a) To produce very small areas of exposure would most likely require very small sources located close to the skin, and the subject would certainly be aware of them; (b) the calculated temperature increases are steady state values, and any small movement of the source with respect to the skin will even out the temperature pattern; (c) for occupational exposures, thermal pain avoidance would prompt an exposed worker to move away from the source of exposure. ICNIRP limits for far infrared energy (whose energy penetration characteristics are similar to those of mm waves) specifies an averaging area of 0.95 cm^2 (11 mm diameter); the limits are designed to protect against burns to a worker from clearly hazardous exposures that are sufficient to cause burns before the worker can move away from the source of exposure. Limits for the general public clearly need to be more conservative (some individuals cannot feel thermal pain).

The 1998 ICNIRP guidelines [currently in force] [1] defined an averaging area of 1 cm^2 with a peak allowable IPD: '*Spatial maximum power densities, averaged over 1 cm^2, should not exceed 20 times the values above*'. This is implicitly intended for a beam with a diameter smaller than 1 cm^2 incident on the body which may be originally taken for non-continuous exposures. In the ICNIRP laser guidelines [30] and draft ANSI laser standard, the aperture of probe (equivalent to diameter of the exposed area of skin) was defined as 11 mm from 300 GHz to 3 THz, which approximately coincides with the area of 1 cm^2 in the draft ICNIRP guidelines.

Assuming that further provisions in the limits are needed to protect against excessive heating from very localized exposures, two different strategies are possible. One is to reduce the averaging area defined in the limits below 1 cm^2, thereby limiting the peak TPD for very small beams (the approach taken in present ICNIRP limits). Attempting to control the peak TPD for very small beams by reducing the averaging area would be inefficient, since it would also limit much less extreme nonuniform beam patterns that will not create excessive heating. A better approach would be to limit the peak TPD or IPD over small areas of skin. Such limits are also included in current ICNIRP guidelines but not in the proposed limits. At present there is almost no experimental data, nor is there evidence that hazardous highly localized exposures are likely to occur with current mm wave technology within current or proposed ICNIRP limit. The issue warrants further examination and experimental data.

In conclusions, the area-averaged TPD is a new and good metric as a surrogate of the surface temperature elevation. The averaging area of 4 cm^2 would be reasonable for frequencies up to 300 GHz provided that they are supplemented by limits on the intensity of very small beams. Alternatively, an averaging area of 1 cm^2 for small beamwidths is a reasonable choice, which also provides continuity with far-infrared guidelines (>300 GHz).

APPENDIX

Fig. 10 shows the permissible output power to satisfy the limits prescribed in ICNIRP 1998, IEEE C95.1-2005, and IPD/TPD for the limit in the ICNIRP public consultation version and IEEE C95.1 draft standard. Note that the limits in the ICNIRP public consultation version and IEEE C95.1 draft standard are the same except for the averaging area; 4cm^2 in the IEEE whereas it is changed at 1 cm^2 in the ICNIRP public consultation document. In the appendix, the averaging area was chosen as 4 cm^2, for simplicity. The limit for TPD and IPD for general public/unrestricted area in the public consultation document and the draft standard are 20 W/m^2 and 55 $f^{-0.177}$ W/m^2 where f is the frequency [GHz]. As shown in Fig. 10, the continuity of the SAR and TPD are 2.6 and 2.3 dB for the dipole antenna and dipole antenna array, respectively, at the transition frequency of 6 GHz, as is similar to Fig. 8. This comparison also suggested that the TPD is generally more conservative than IPD but it was not true

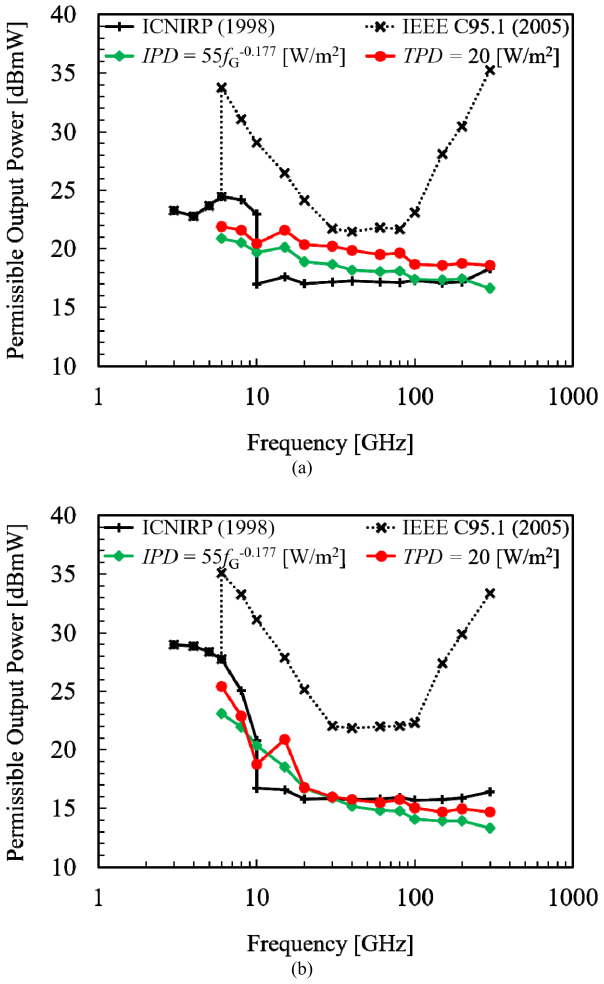

FIGURE 10. Permissible output power for (a) dipole antenna and (b) dipole antenna array for ICNIRP 1998, IEEE C95.1-2005, and IPD/TPD averaged over 4 cm^2 for the limit in the ICNIRP public consultation version and IEEE C95.1 draft standard.

for the dipole array at 10 GHz, due to the antenna-human coupling.

Colombi *et al.* [31] pointed out a drastic change of the maximum permissible output power of antennas near tissue surfaces to remain compliant with present MPE limits of different standards above and below the transition frequency (3-10 GHz). However, for the metrics shown in the revised limits (ICNIRP public consultation document and IEEE C95.1 draft standard), the change at the transition is smaller than -2.6 dB, though only a limited number of antennas were considered here. The reason for this gap is that the TPD limit in the draft guidelines/standard are derived in a conservative manner using 1-D analysis. However, this difference at the transition frequency is much smaller than that of the current ICNIRP and IEEE.

REFERENCES

[1] A. Ahlbom *et al.*, "Guidelines for limiting exposure to time-varying electric, magnetic, and electromagnetic fields (up to 300 GHz)," *Health Phys.*, vol. 74, no. 4, pp. 494–521, 1998.

[2] *IEEE Standard for Safety Levels with Respect to Human Exposure to Radio Frequency Electromagnetic Fields, 3 kHz to 300 GHz*, IEEE Standard C95.1-2005, New York, NY, USA, 2005.

[3] *IEEE Standard for Military Workplaces—Force Health Protection Regarding Personnel Exposure to Electric, Magnetic, and Electromagnetic Fields, 0 Hz to 300 GHz*, IEEE Standard C95.1-2345, 2014.

[4] A. Hirata and T. Shiozawa, "Correlation of maximum temperature increase and peak SAR in the human head due to handset antennas," *IEEE Trans. Microw. Theory Techn.*, vol. 51, no. 7, pp. 1834–1841, Jul. 2003.

[5] A. Hirata and O. Fujiwara, "The correlation between mass-averaged SAR and temperature elevation in the human head model exposed to RF near-fields from 1 to 6 GHz," *Phys. Med. Biol.*, vol. 54, no. 23, pp. 7227–7238, 2009.

[6] A. Razmadze, L. Shoshiashvili, D. Kakulia, R. Zaridze, G. Bit-Babik, and A. Faraone, "Influence of specific absorption rate averaging schemes on correlation between mass-averaged specific absorption rate and temperature rise," *Electromagnetics*, vol. 29, no. 1, pp. 77–90, 2009.

[7] R. L. McIntosh and V. Anderson, "SAR versus Sinc: What is the appropriate RF exposure metric in the range 1–10 GHz? Part II: Using complex human body models," *Bioelectromagnetics*, vol. 31, no. 6, pp. 467–478, 2010.

[8] K. R. Foster, M. C. Ziskin, and Q. Balzano, "Thermal response of human skin to microwave energy: A critical review," *Health Phys.*, vol. 111, no. 6, pp. 528–541, 2016.

[9] Y. Hashimoto *et al.*, "On the averaging area for incident power density for human exposure limits at frequencies over 6 GHz," *Phys. Med. Biol.*, vol. 62, no. 8, p. 3124, 2017.

[10] K. Sasaki, M. Mizuno, K. Wake, and S. Watanabe, "Monte Carlo simulations of skin exposure to electromagnetic field from 10 GHz to 1 THz," *Phys. Med. Biol.*, vol. 62, no. 17, p. 6993, 2017.

[11] T. Nagaoka *et al.*, "Development of realistic high-resolution whole-body voxel models of Japanese adult males and females of average height and weight, and application of models to radio-frequency electromagnetic-field dosimetry," *Phys. Med. Biol.*, vol. 49, no. 1, pp. 1–15, 2004.

[12] K. Taguchi, T. Kashiwa, and A. Hirata, "Development on high resolution human voxel model for high frequency exposure analysis," presented at the Rrog. Electromagn. Res. Symp., Toyama, Japan, 2018.

[13] A. Taflove and S. C. Hagness, *Computational Electrodynamics: The Finite-Difference Time-Domain Method*, 3rd ed. Northwood, MA, USA: Artech House, 2005.

[14] S. Gabriel, R. W. Lau, and C. Gabriel, "The dielectric properties of biological tissues: III. Parametric models for the dielectric spectrum of tissues," *Phys. Med. Biol.*, vol. 41, no. 11, pp. 2271–2293, 1996.

[15] K. Sasaki, K. Wake, and S. Watanabe, "Development of best fit Cole-Cole parameters for measurement data from biological tissues and organs between 1 MHz and 20 GHz," *Radio Sci.*, vol. 49, no. 7, pp. 459–472, Jul. 2014.

[16] K. Sasaki, K. Wake, and S. Watanabe, "Measurement of the dielectric properties of the epidermis and dermis at frequencies from 0.5 GHz to 110 GHz," *Phys. Med. Biol.*, vol. 59, no. 16, p. 4739, 2014.

[17] M. C. Ziskin, S. I. Alekseev, K. R. Foster, and Q. Balzano, "Tissue models for RF exposure evaluation at frequencies above 6 GHz," *Bioelectromagnetics*, vol. 39, no. 3, pp. 173–189, 2018.

[18] R. Morimoto, I. Laakso, V. De Santis, and A. Hirata, "Relationship between peak spatial-averaged specific absorption rate and peak temperature elevation in human head in frequency range of 1–30 GHz," *Phys. Med. Biol.*, vol. 61, no. 14, p. 5406, 2016.

[19] H. H. Pennes, "Analysis of tissue and arterial blood temperatures in the resting human forearm," *J. Appl. Physiol.*, vol. 1, no. 2, pp. 93–122, 1948.

[20] I. Laakso, "Assessment of the computational uncertainty of temperature rise and SAR in the eyes and brain under far-field exposure from 1 to 10 GHz," *Phys. Med. Biol.*, vol. 54, no. 11, p. 3393, 2009.

[21] F. A. Duck, *Physical Properties of Tissues: A Comprehensive Reference Book*. New York, NY, USA: Academic, 1990.

[22] P. Hasgall *et al.*, "IT'IS database for thermal and electromagnetic parameters of biological tissue," Version 3.0, Sep. 2015. [Online]. Available: www.itis.ethz.ch/database, doi: 10.13099/VIP21000-03-0.

[23] I. Laakso, R. Morimoto, A. Hirata, and T. Onishi, "Computational dosimetry of the human head exposed to near-field microwaves using measured blood flow," *IEEE Trans. Electromagn. Compat.*, vol. 59, no. 2, pp. 739–746, Apr. 2017.

[24] S. Kodera, J. Gomez-Tames, and A. Hirata, "Temperature elevation in the human brain and skin with thermoregulation during exposure to RF energy," *BioMedical Eng. OnLine*, vol. 17, p. 1, Jan. 2018.

[25] K. R. Foster, M. C. Ziskin, and Q. Balzano, "Thermal modeling for the next generation of radiofrequency exposure limits: Commentary," *Health Phys.*, vol. 113, no. 1, pp. 41–53, 2017.

[26] K. R. Foster, M. C. Ziskin, Q. Balzano, and G. Bit-Babik, "Modeling tissue heating from exposure to radiofrequency energy and relevance of tissue heating to exposure limits: heating factor," *Health Phys.*, vol. 115, no. 2, pp. 295–307, 2018.
[27] K. M. Mak, H. W. Lai, and K. M. Luk, "A 5G wideband patch antenna with antisymmetric L-shaped probe feeds," *IEEE Trans. Antennas Propag.*, vol. 66, no. 2, pp. 957–961, Feb. 2018.
[28] D. Colombi, B. Thors, C. Törnevik, and Q. Balzano, "RF energy absorption by biological tissues in close proximity to millimeter-wave 5G wireless equipment," *IEEE Access*, vol. 6, pp. 4974–4981, 2018.
[29] K. R. Foster, M. C. Ziskin, Q. Balzano, and A. Hirata, "Thermal analysis of averaging times in radiofrequency exposure limits above 1 GHz," *IEEE Access*, to be published, doi: 10.1109/ACCESS.2018.2883175.
[30] International Commission on Non-Ionizing Radiation Protection, "ICNIRP guidelines on limits of exposure to laser radiation of wavelengths between 180 nm and 1,000 μm," *Health Phys.*, vol. 105, no. 3, pp. 271–295, 2013.
[31] D. Colombi, B. Thors, and C. Törnevik, "Implications of EMF exposure limits on output power levels for 5G devices above 6 GHz," *IEEE Antennas Wireless Propag. Lett.*, vol. 14, pp. 1247–1249, 2015.

DAISUKE FUNAHASHI received the B.E. degree in electrical and electronic engineering from the Nagoya Institute of Technology, Nagoya, Japan, in 2017, where he is currently pursuing the master's degree in electrical and mechanical engineering.

His current research focuses on human protection from electromagnetic field at radio frequency.

AKIMASA HIRATA (S'98–M'01–SM'10–F'17) received the B.E., M.E., and Ph.D. degrees in communications engineering from Osaka University, Suita, Japan, in 1996, 1998, and 2000, respectively.

From 1999 to 2001, he was a Research Fellow of the Japan Society for the Promotion of Science. He was also a Visiting Research Scientist at the University of Victoria, Victoria, BC, Canada, in 2000. In 2001, he joined the Department of Communications Engineering, Osaka University, as an Assistant Professor. In 2004, he joined the Department of Computer Science and Engineering, Nagoya Institute of Technology, as an Associate Professor, where he is currently a Full Professor. His research interests include electromagnetic safety, risk management system for heat-related illness, methods in neuroscience, antennas, filters, and related computational techniques.

Dr. Hirata is a fellow of the Institute of Physics, and a member of IEICE, IEE Japan, and the Bioelectromagnetics Society. He is an Editorial Board Member of *Physics in Medicine and Biology*, a member of the main commission, the Chair of the Project Group of the International Commission on Non-Ionizing Radiation Protection, a member of administrative committee, a Subcommittee (EMF Dosimetry Modeling) Chair of the IEEE International Committee on Electromagnetic Safety, and an expert of the World Health Organization. He received several awards, including the Young cientists' Prize (2006) and the Prizes for Science and Technology (Research Category 2011 and Public Understanding Promotion Category 2014) by the Commendation for Science and Technology by the Minister of Education, Culture, Sports, Science, and Technology, Japan, and the IEEE EMC-S Technical Achievement Award (2015), and the Japan Academy Medal and JSPS Prize (2018). From 2006 to 2012, he was an Associate Editor of the IEEE TRANSACTIONS ON BIOMEDICAL ENGINEERING.

SACHIKO KODERA received the B.E. and M.E. degrees in electrical and computer engineering from the Nagoya Institute of Technology, Nagoya, Japan, in 2002 and 2006, respectively.

In 2016, she joined the Department of Electrical and Mechanical Engineering, Nagoya Institute of Technology, as a Researcher. Her current research interests include electromagnetic and thermal dosimetry modeling in humans for radiofrequency and ambient heat exposures.

KENNETH R. FOSTER (M'77–SM'81–F'88–LF'13) received the Ph.D. degree in physics from Indiana University Bloomington, Bloomington, IN, USA, in 1971. He was with the U.S. Navy, Naval Medical Research Institute, Bethesda, MD, USA, from 1971 to 1976. Since 1976, he has been with the Department of Bioengineering, University of Pennsylvania, Philadelphia, PA, USA, where he is currently a Professor Emeritus. He has been involved in studies on the interaction of nonionizing radiation and biological systems, including mechanisms of interaction and biomedical applications of radio frequency and microwave energy. In addition, he has written widely about scientific issues related to possible health effects of electromagnetic fields. He has authored approximately 160 technical papers in peer-reviewed journals, numerous other articles, and two books related to technological risk and the law. In 2016, he received the d'Arsonval Award from the Bioelectromagnetics Society for contributions to the field of bioelectromagnetics. He has been active for many years on the IEEE EMBS Committee of Man and Radiation, the IEEE Society on Social Implications of Technology, and the IEEE Engineering in Medicine and Biology Society. He is a long-time Member of TC 95 of the IEEE International Committee on Electromagnetic Safety and a member of the Physical Agents Committee of the American Conference of Industrial Hygienists, among many other professional activities. He is the co-Editor-in-Chief of *BioMedical Engineering Online*.